

RESEARCH ARTICLE

10.1029/2018JD028830

Key Points:

- Model of polar mesospheric cloud (PMC) effects on mesospheric chemistry
- Seasonal depletion of hydrogen at 95 km due to PMC condensation and associated dehydration
- Effects seen at latitudes away from the PMC region, at higher altitudes up into the thermosphere as well as in a localized ozone enhancement

Correspondence to:

D. E. Siskind,
david.siskind@nrl.navy.mil

Citation:


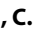
Siskind, D. E., Merkel, A. W., Marsh, D. R., Randall, C. E., Hervig, M. E., Mlynczak, M. G., & Russell, J. M. III (2018). Understanding the effects of polar mesospheric clouds on the environment of the upper mesosphere and lower thermosphere. *Journal of Geophysical Research: Atmospheres*, 123. <https://doi.org/10.1029/2018JD028830>

Received 16 APR 2018

Accepted 21 SEP 2018

Accepted article online 28 SEP 2018

Understanding the Effects of Polar Mesospheric Clouds on the Environment of the Upper Mesosphere and Lower Thermosphere

David E. Siskind¹ , A. W. Merkel² , D. R. Marsh³ , C. E. Randall² , M. E. Hervig⁴ , M. G. Mlynczak⁵ , and J. M. Russell III⁶

¹Space Science Division, Naval Research Laboratory, Washington, DC, USA, ²Laboratory for Atmospheric and Space Physics, University of Colorado Boulder, Boulder, CO, USA, ³National Center for Atmospheric Research, Boulder, CO, USA, ⁴GATS Inc., Driggs, ID, USA, ⁵NASA Langley Research Center, Hampton, VA, USA, ⁶Center for Atmospheric Sciences, Hampton University, Hampton, VA, USA

Abstract This study focuses on the effects of polar mesospheric cloud (PMC) formation on the chemical environment of the mesosphere and lower thermosphere. Of specific interest is how the dehydration due to mesospheric ice particle formation leads to significant seasonal decreases in the atomic hydrogen near the mesopause at middle to high latitudes. Using a three-dimensional whole atmosphere coupled chemistry/dynamics model, we simulate the effects of this dehydration, and via comparisons with three data sets taken from two NASA satellites, we quantify the perturbations to atomic hydrogen and water vapor. We also identify a local ozone maximum that results from the PMC-induced decrease in atomic hydrogen. Further, the large interannual variability in the onset of the Southern Hemisphere PMC season correlates well with the interannual variability of early summer atomic hydrogen at 95 km. Since the PMC onset is known to be controlled by interannual variations in the Southern Hemisphere stratospheric polar vortex, this correlation indicates a coupling between the stratosphere and the chemistry of the mesosphere and lower thermosphere. Finally, our model results suggest that the seasonal biteout in atomic hydrogen propagates up into the thermosphere and to lower latitudes. This raises the intriguing possibility that PMC formation might play a role in modulating the escape of hydrogen from the atmosphere.

Plain Language Summary Polar mesospheric clouds (PMCs) are Earth's highest clouds (82 km altitude). They consist of nanometer-sized ice crystals nucleated onto meteoric smoke particles. When these clouds are formed, they dehydrate the surrounding atmosphere and when these clouds sublimate, they release the water vapor back into the surrounding environment. These patterns of condensation and sublimation are observed from NASA satellites and we model these data with a general circulation model. We quantify the effects that they have on the chemistry of the atmosphere at the edge of space. Our results show that it is possible that PMC condensation could affect the flow of hydrogen upward into the upper atmosphere.

1. Introduction

The unusual and extreme conditions that characterize the cold summer polar mesopause have motivated decades of work to understand how polar mesospheric clouds (PMCs) are indicators of that environment. From these studies, we now understand that PMCs respond in a complex way to both dynamical variability propagating up from the lower and middle atmosphere (France et al., 2018; Karlsson et al., 2007, 2009, 2011; Merkel, Rusch, et al., 2009; Siskind et al., 2011; Siskind & McCormack, 2014) as well as solar forcing from above (DeLand et al., 2003; Garcia, 1989; Hervig & Siskind, 2006; Hervig & Stevens, 2014; Thurairajah et al., 2017). Satellite observations showing marked increases in PMC brightness (DeLand & Thomas, 2015) and frequency (Shettle et al., 2009) are at least partially consistent with mesopause temperature and humidity changes from anthropogenic effects such as increasing CO₂ and CH₄ (Hervig et al., 2016; Lubken et al., 2009). However, uncertainties remain; for example, the specific contributions from anthropogenic effects have not been well quantified and the PMC response to recent solar cycle activity variability appears to have been less than expected (Hervig et al., 2016; Siskind, Stevens, Hervig, et al., 2013). These uncertainties continue to motivate much of the current research on PMCs.

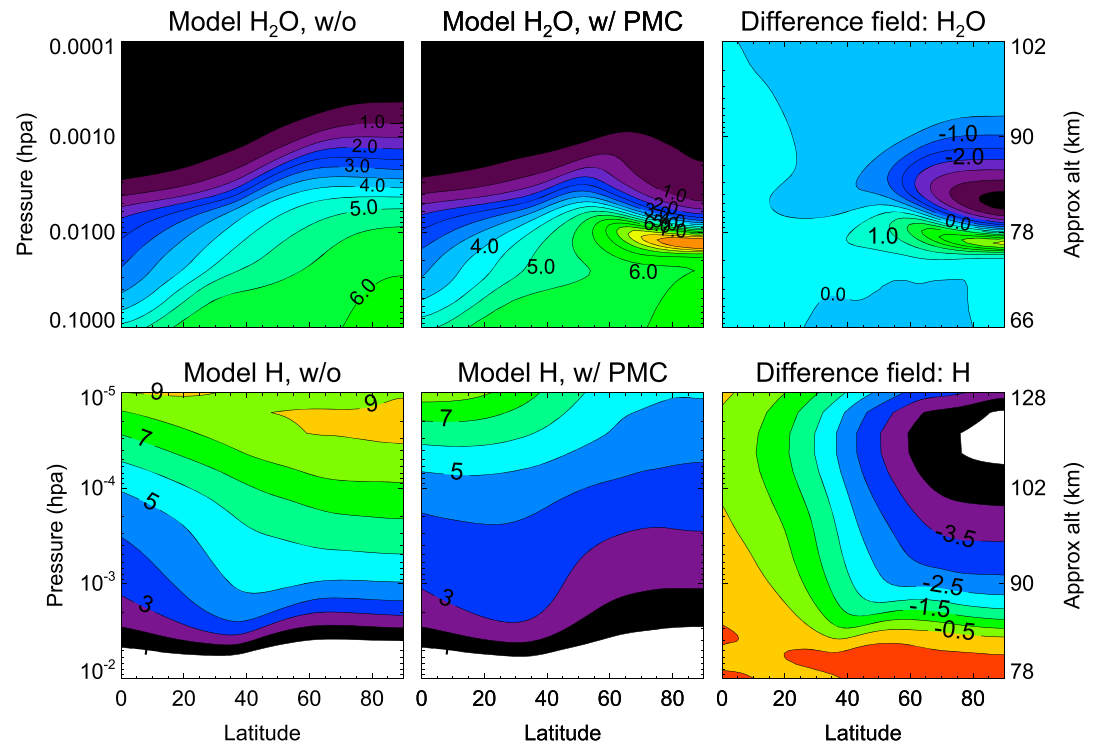


Figure 1. Model water vapor (top row) and atomic hydrogen (bottom) representing a July monthly averaged zonal mean calculated from 8 model years. The left column is a control run that does not include PMCs, the middle column is with the PMC parameterization, and the right column is the difference. Approximate altitude scales from the model geopotential heights are given on the right. Note that the pressure ranges and associated altitudes are different for the H_2O and H plots. PMC = polar mesospheric cloud.

The converse question has also become of interest, namely, how might PMCs actively influence their environment? For example, there have been both model (Bardeen et al., 2010; von Zahn & Berger, 2003) and observational (Hervig et al., 2003, 2015; Summers et al., 2001,) reports of significant perturbations to the water vapor distribution from PMC formation. The PMC influence on mesospheric water vapor is presumably due to dehydration by condensing ice particles as well as from sublimation when ice particles sediment into warmer air. We have also reported that the atomic hydrogen observed from the Sounding of the Atmosphere using Broadband Emission Radiometry (SABER) instrument on the Thermosphere Ionosphere Mesosphere Energetics and Dynamics (TIMED) satellite decreases during the high latitude summer and have interpreted this decrease as an indicator of dehydration due to the condensation of water vapor into ice from PMC formation (Siskind et al., 2008). Here we expand upon that hypothesis and take a comprehensive look at how PMCs might influence the chemical environment of the mesosphere and lower thermosphere. We do this with a three-dimensional whole atmosphere model that includes a parameterization for PMC formation. We compare these model results with data from both SABER and the Aeronomy of Ice in the Mesosphere (AIM) Small Explorer mission. Section 2 describes the model and observations, section 3 presents model-measurement comparisons illustrating how PMC formation affects the chemical environment that extends into the thermosphere. It also presents new details concerning nighttime mesospheric ozone variability as well as coupling with stratospheric interannual variability. Section 4 is the conclusion.

2. Analysis Approach

2.1. The WACCM-PMC Model

The Whole Atmosphere Community Climate Model (WACCM) is a fully coupled chemistry, radiation, and dynamics global model extending from the surface to the thermosphere (Garcia et al., 2007). WACCM-PMC incorporates a bulk parameterization of ice particle microphysics to simulate PMCs as first described by Merkel, Marsh, et al., (2009). The use of a bulk parameterization facilitates long simulations as compared with the more detailed but resource-intensive approach that uses the Community Aerosol and Radiation Model for Atmospheres (Bardeen et al., 2010). WACCM-PMC allows for a representation of ice cloud microphysics

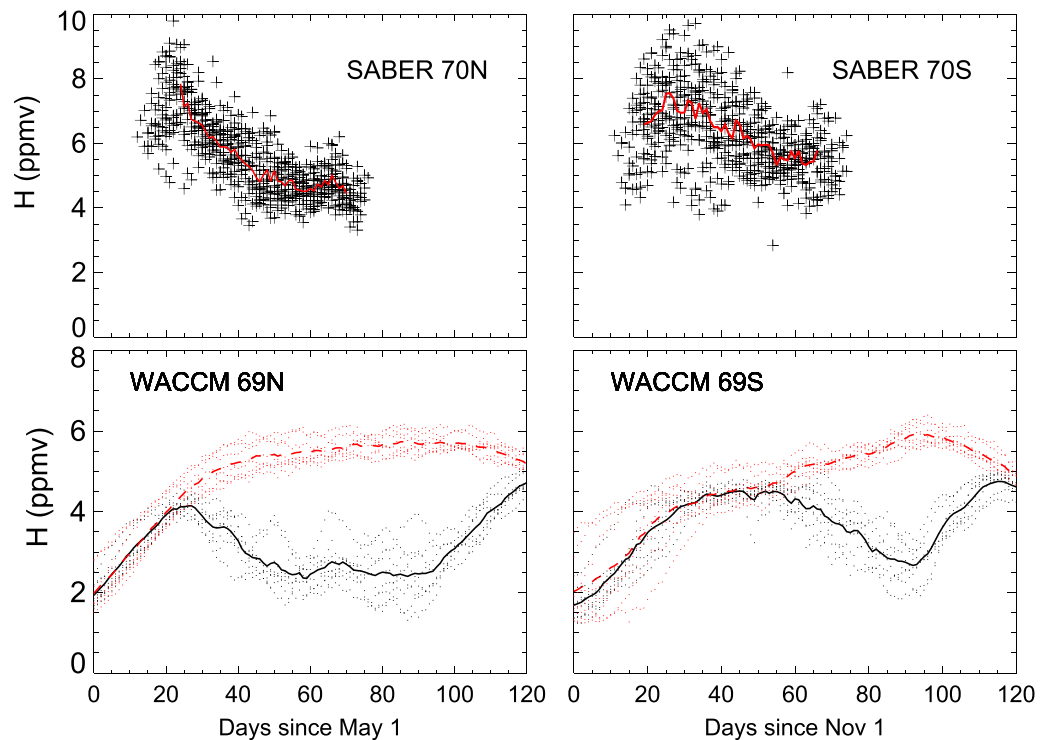


Figure 2. Comparison of SABER H variation (top row) for 70°N and 70°S at .0006 hPa (near 94 km) with WACCM (bottom row). The y axes are mixing ratio. For the SABER data, 12 years of data are shown (plus symbols); the red curve is the average over the period where SABER was commonly yawed to view the polar regions. This varied from year to year and thus the average does not span the entire period. For the WACCM results, the red is the control case without polar mesospheric clouds included, black is with polar mesospheric clouds. The dots are individual daily averages for each of 8 model years. The thick black line is the 8-year average. SABER = Sounding of the Atmosphere using Broadband Emission Radiometry; WACCM = Whole Atmosphere Community Climate Model.

including the simulation of particle growth, sublimation, and sedimentation. The microphysical process of PMC formation (Q) can be thought of as being the sum of two processes (nucleation and growth): $Q = Q_{nuc} + Q_{growth}$. In WACCM-PMC Q_{nuc} is parameterized. Following and extending the approach of Siskind et al. (2007), we assume nucleation occurs only when the saturation ratio (S), defined as the water vapor partial pressure over the saturation pressure of water over ice (p_{sat}), is greater than 30. When the local environment is supersaturated, a small percentage of the available water vapor is converted to ice. The model does not consider the distribution of nucleation particles such as meteoric smoke particles (Megner et al., 2008). Once the ice is nucleated, the calculation of growth/sublimation is straightforward, but depends on the effective radius of the ice particle. Instead of keeping track of each ice particle, WACCM-PMC uses a parameterization that estimates the radius based on the local temperature and ice water content (IWC) through an empirical formula. Merkel, Marsh, et al., (2009) validated the relationship between these three variables in WACCM-PMC by detailed comparisons with data from the AIM Solar Occultation for Ice Experiment (SOFIE; Gordley et al., 2009; Hervig et al., 2009). As compared with SOFIE, WACCM-PMC accurately represents the phase transitions between water vapor and ice, and therefore reliably simulates the dehydration caused by PMCs. Further, since WACCM is run with a fully interactive chemistry module, the redistribution of water vapor in the PMC region will feed back into the local chemical composition. One consideration with our use of WACCM-PMC, which is based on WACCM version 3 (V3), is that the WACCM model has evolved since Merkel, Marsh, et al., (2009). Specifically, improvements have been made to the formulation of gravity wave drag (e.g., Richter et al., 2010); however, even with these improvements, problems have been identified (Garcia et al., 2017). We note that while Bardeen et al. (2016) used WACCM version 4 in their latest simulations with Community Aerosol and Radiation Model for Atmospheres, they nonetheless retained the gravity wave parameterization from WACCM V3 since it was better tuned to reproduce conditions at the summer mesopause. Possible consequences of deficiencies in the WACCM gravity wave scheme will be discussed further below.

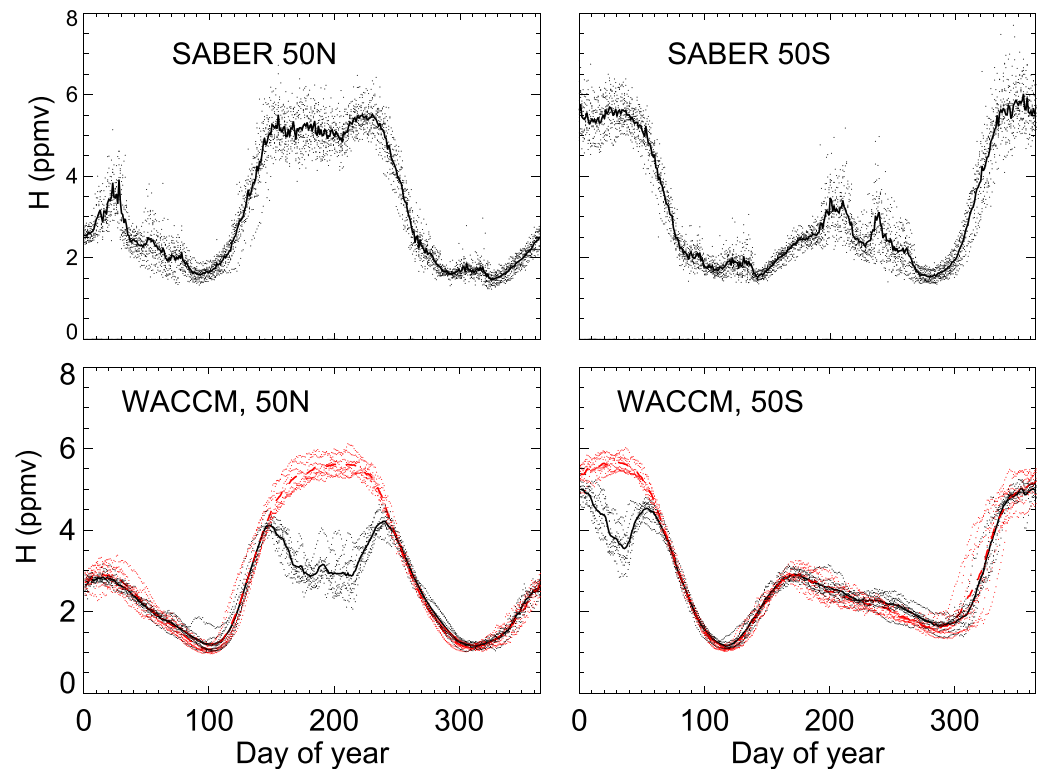


Figure 3. Same comparison as Figure 2, but for 50°N and 50°S. Because SABER samples these latitudes year round, we show a full annual cycle for both data and model. The heavy black line in the two SABER panels is a 12-year average. SABER = Sounding of the Atmosphere using Broadband Emission Radiometry; WACCM = Whole Atmosphere Community Climate Model.

We compare two cases of WACCM-PMC, a control run with the PMC parameterization disabled (no PMC formation) and a case with the parameterization enabled (with PMC formation). Each case is perpetually run for 10 model years, with the same annual forcing using fixed solar input representative of 2003 (i.e., medium) levels. The first 2 years were discarded to avoid any possible spin-up problems and so only results from the 8 years of model data are shown. These 8 years are averaged to produce a representative average model year for each case. Figure 1 illustrates the modeled zonal mean H_2O (top row) and atomic hydrogen H (bottom row) for the month of July. The left column represents the control case (no PMC formation), the middle column represents the case with PMCs, and the right column shows the difference between the two cases. An approximate altitude scale based upon the model geopotential height field is also given on the right for the two sets of plots. The figure shows that without PMCs, atomic hydrogen increases as water vapor decreases as a function of altitude to near the top of the model ($p = 10^{-5}$ hPa, approximately 128 km). In addition, for a given altitude, both H_2O and H increase with increasing latitude. This reflects the well-known summertime upwelling of water vapor following the mean meridional circulation, which maximizes at high latitudes (Qian et al., 2018). When PMCs are considered, there is a noticeable perturbation to the H_2O field such that above about .006 hPa, the high latitude H_2O is depleted, while right below 0.01 hPa there is a thin layer of enhanced H_2O from sublimating PMCs. The H_2O perturbation is reflected in a marked change in the H field such that the equator-to-pole latitude gradient is reversed (bottom middle panel); H now is largest at the equator. The difference fields highlight the effects of dehydration and sublimation and show that the entire hemisphere of atomic hydrogen above $p = .001$ hPa is reduced in the PMC case relative to the control case (bottom right panel). The model simulations demonstrate that PMC formation is expected to affect the distribution of atomic hydrogen throughout the global mesosphere and lower thermosphere region. In the sections that follow, we will make detailed comparisons of the model results with observations.

2.2. Satellite Data: SABER, SOFIE, and CIPS

We bring together mesospheric and lower thermosphere data taken from three different instruments on two NASA satellites, TIMED and AIM. From TIMED-SABER, we use the temperature, ozone, and atomic hydrogen

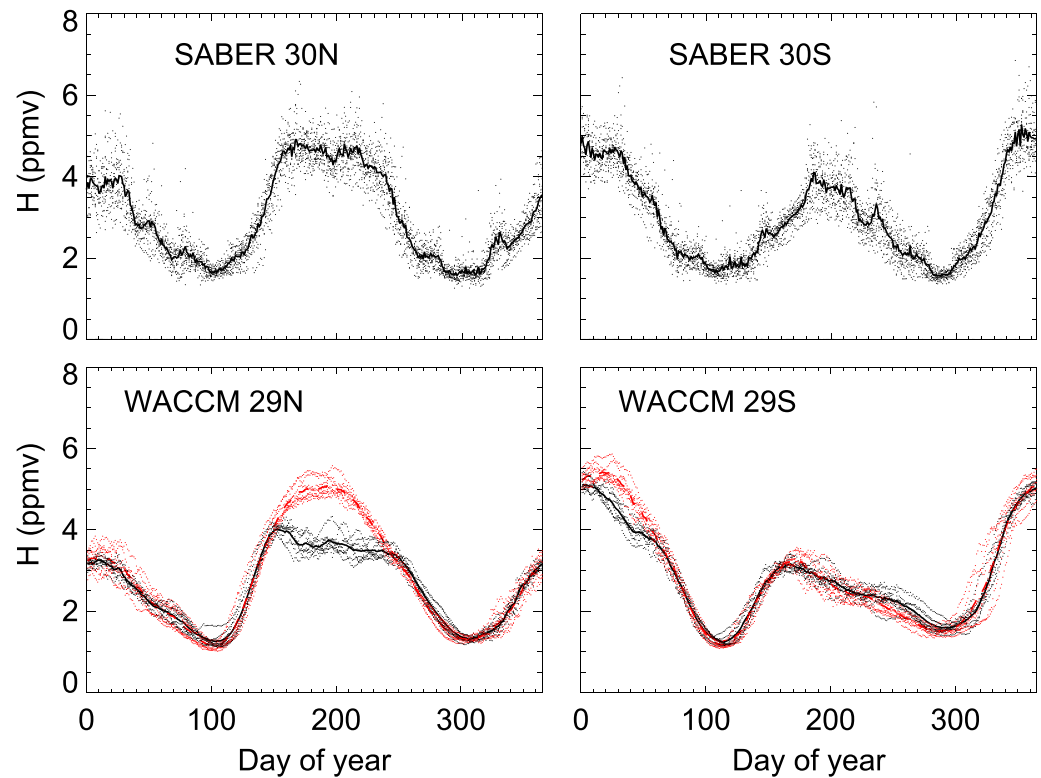


Figure 4. Same as Figure 3, but for 30°N and 30°S. SABER = Sounding of the Atmosphere using Broadband Emission Radiometry; WACCM = Whole Atmosphere Community Climate Model.

data. The temperature data are described by Remsberg et al. (2008). The ozone measurements and comparisons with other data are discussed by Rong et al. (2009) and Smith et al. (2013). Those papers used V1.07; here we use V2 (e.g., Smith et al., 2018). The main difference between the two data versions is in the temperature retrieval algorithm, which necessarily underlies the constituent retrievals. The derivation of the H abundance is based upon both the ozone data and measurements of the vibrationally excited hydroxyl airglow; this is discussed in depth by Mlynczak et al. (2013). Mlynczak et al. (2018) provide some updates to this retrieval; however, we did not use this very latest retrieval. This is because (1) it is only available at night and we wish to compare directly with PMC data in polar summer and (2) Mlynczak et al. (2013) speculate that if future ozone retrievals change, this latest atomic oxygen retrieval might not be the final word on SABER H .

From AIM, we used IWC from SOFIE, which has been shown to be a useful measure of the amount of water vapor sequestered into PMCs (Stevens et al., 2007) and which can be readily compared with our model results. In addition, we used SOFIE water vapor profile measurements (Rong et al., 2010). SOFIE is however limited to specific occultation latitudes, which began to drift after 2013, especially in the Southern Hemisphere (SH). Therefore, we also compare to data from the AIM Cloud Imaging and Particle Size (CIPS; Bailey et al., 2009; Lumpe et al., 2013; Rusch et al., 2009) instrument, which provides a more extended climatology of PMC occurrence frequency.

3. Model/Data Comparisons

3.1. H , H_2O , and PMCs

As mentioned, Siskind et al. (2008) showed that high latitude H (as observed from SABER) decreased as the summer progressed instead of increasing as simple models suggested. This variation was interpreted as dehydration due to PMC formation. Figure 2 presents updated SABER H based upon the reprocessing discussed by Mlynczak et al. (2013) and compares it with our WACCM-PMC case study runs. The top row of Figure 2 shows a summary of 12 years (2002–2013) of H data, at .0006 hpa (near 94–95 km), in late spring and early summer for both hemispheres. The bottom row shows corresponding results from the model. Note that one limitation of SABER is that it does not always observe latitudes poleward of 50°. Rather it yaws approximately every

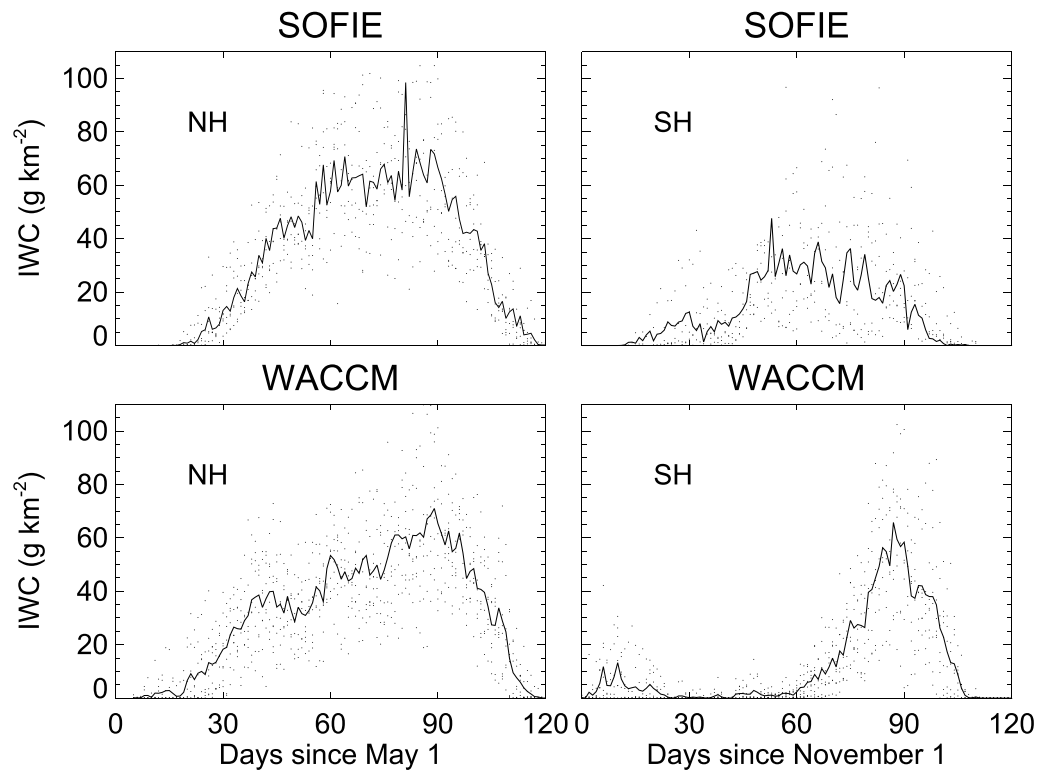


Figure 5. Column ice abundance from SOFIE (top row) compared with WACCM-PMC. SOFIE latitudes range from near 65°N or S at summer solstice (approximately Day 50 on each plot), rising to about 72°N (S) by early August (February) and WACCM-PMC is sampled accordingly. The WACCM-PMC results are daily averages from 8 model years and the 8-year average (black curve). The SOFIE data are daily averaged from 6 years of data (2008–2013) for the NH and 5 years of data (2007/08–2011/12) for the SH. The multiyear average is the black curve. IWC = ice water content; SOFIE = Solar Occultation for Ice Experiment; WACCM = Whole Atmosphere Community Climate Model; PMC = polar mesospheric cloud.

2 months such that at any one time it covers about 130° of latitude from 80° in a given hemisphere to 50° in the opposite one. Thus, there are two periods where SABER sees into the PMC formation region, one from mid-May to mid-July in the Northern Hemisphere (NH) and the other from mid-November to mid-January in the SH. Each panel of SABER data shows a solid red line that is the 12-year average. This average does not completely cover all the data shown because the period of the yaw varies from year to year and thus the period where data are available for all 12 years is a subset of the total number of observations. During both periods there is a suggestion of a 1- to 2-week period at the beginning of the yaw where the H is increasing, followed by a sharp decrease starting around 25 May for the NH and 25 November for the SH. These dates coincide with the general beginning of the PMC season (Benze et al., 2012; Siskind et al., 2015). It is interesting to note that the net decrease is less in the SH relative to the NH (from 7.5 to 5.5 ppmv in the SH compared with 7.5 to 4.5 ppmv in the NH). Furthermore, there is more scatter in the SH hydrogen; for example, there is a cluster of points late in the spring season (Day 30) that are already lower than the average value seen after Day 60 (1 January). These N/S differences correspond to known hemispheric differences in PMC abundance and season onset and will be discussed further when we compare with model PMC results.

The bottom of Figure 2 shows corresponding model results both for a control run without PMCs and the run with PMCs. The figure shows both the multiyear average and individual daily averaged results. Despite some year-to-year scatter, the model clearly shows that with PMCs considered, there is an abrupt decrease in H beginning around 25 days from 1 May in the NH, almost exactly as in the data. Without PMCs, there is a midsummer maximum in H . The magnitude of the H decrease in both the model and in the SABER data is about a factor of 2 in the NH. In the SH, there is still a marked H decrease; however, there is a noticeable delay of about a month in the model relative to the observations. This is a persistent feature of our model results and is likely due to a long-recognized problem in WACCM whereby the breakdown of the SH stratospheric vortex in the model is delayed relative to climatology (Garcia et al., 2017). As discussed by Smith et al. (2010)

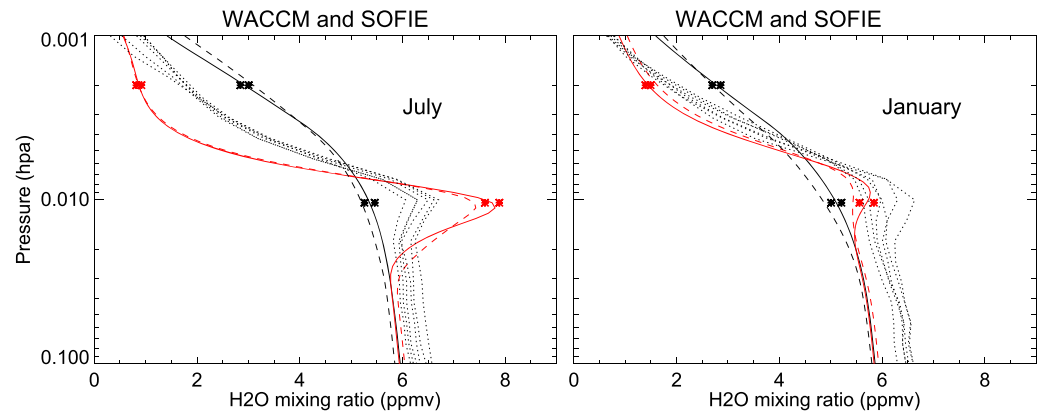


Figure 6. Comparison of monthly averaged WACCM H₂O (July for NH, January for SH) with SOFIE. The latitudes are between 67° and 71°. The thick black curve is the average WACCM solution without polar mesospheric clouds. The stars at 0.002 and .01 hPa are a measure of the spread of the 8 model years that went into the average. The red curves represent averages of two simulations (with the polar mesospheric clouds) with different Pr numbers. The solid red curve is the standard case (Pr = 4); the dashed red curve is with Pr = 2 (i.e., doubled K_{zz}). The black dotted curves are individual years of SOFIE. Monthly averages from 2007 to 2013 are shown. WACCM = Whole Atmosphere Community Climate Model; SOFIE = Solar Occultation for Ice Experiment; Pr = Prandtl.

the breakdown of the vortex is important for PMC formation because it allows the transmission of gravity waves that cool the summer mesopause. This link between vortex breakdown and PMC onset only holds for the SH because the breakdown can be delayed until near summer solstice. A consequence of the SH delay in the model is that while the peak magnitude of the H depletion in the SH is similar to the NH, the duration of the reduced H is much shorter in the SH (about 40–50 days) compared with the NH (about 90–100 days).

Figures 3 and 4 extend the comparison in Figure 2 to lower latitudes where continuous year round observations are possible from SABER. Figure 3 is for 50° and Figure 4 is for 30°, with the data in the top row and WACCM in the bottom row for both figures. Interestingly, even at these lower latitudes, away from the core PMC region, there appears to be a clear discontinuity in the seasonal variation of H such that the springtime increase appears to abruptly stop at the beginning of June (Day 150) in the NH. The fact that this occurs even at 30°N suggests the effects of PMC dehydration can spread to latitudes well away from the summer polar region. We interpret this as due to the mean meridional circulation, which is equatorward at these altitudes and for this time of year (Smith et al., 2011). Qian et al. (2018) discuss in detail the relative roles of diffusion and advection governing the distribution of H in the lowermost thermosphere. The seasonal discontinuity is evident at 50°S but not at 30°. Again, this is consistent with fewer PMCs in the SH relative to the NH. It appears that WACCM somewhat overestimates the summer biteout at 50°, but is in very good agreement at 30°.

Figure 5 shows the calculated height integrated ice mass (i.e., IWC) from SOFIE (top row) compared with the WACCM-PMC case that includes PMCs (bottom row). The solid lines in each panel represent multiyear averages, which were calculated from a 6-year average (2008–2013) for SOFIE in the NH, a 5-year average (August 2007 to December 2011) for SOFIE in the SH, and the same 8-year average for WACCM-PMC discussed above. In addition, the scatter points show the individual daily averages for both SOFIE and WACCM-PMC. In general, the agreement between model and data is very good. For both SOFIE and WACCM-PMC, the NH IWC begins to increase in late May (Days 20–30), shows an apparent plateau in IWC during June, jumps up by about 20% around Day 55 (late June), and peaks around Day 85 (late July). The occurrence of peak IWC in late July partly reflects the fact that the latitudes of the SOFIE occultations are somewhat higher in late July (72°N) compared with solstice (66°N) and thus correspond to a region where IWC is normally greater (e.g., Garcia-Comas et al., 2016). The magnitude of the peak (65–70 g/km²) also agrees well between model and data.

As with the SABER atomic hydrogen, there are several important North/South differences seen in the SOFIE data in Figure 5. First, the overall IWC values are lower in the SH. This reflects the well-known pattern whereby PMCs are less abundant in the SH due to interhemispheric differences in middle atmospheric dynamics (Bailey et al., 2005; Garcia-Comas et al., 2016; Hervig et al., 2013; Siskind et al., 2003). Second, there is greater scatter in the SH IWC values such that, even in midseason, there are numerous individual IWC points below 10 g/km², while in the NH there is roughly a 50-day period where SOFIE never sees IWC below 15 g/km². Finally, the

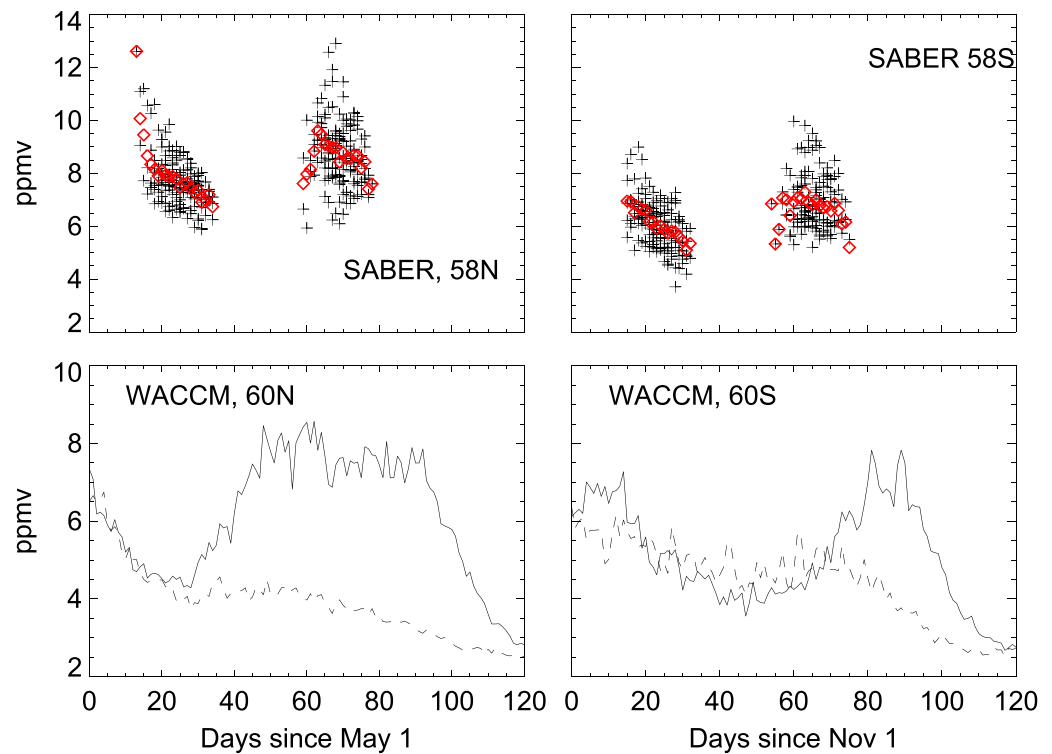


Figure 7. Time series of SABER nighttime ozone (top row) for the years 2002–2013 and concomitant WACCM results (bottom). The left column is NH, the right is SH. The SABER data are zonal averages between 56° and 60° from the equator for a pressure of 0.0075 hPa (about 91–93 km). Because of changing local times, SABER does not acquire continuous nighttime data, but for this yaw cycle, observes near 23:00 local time at the beginning of the period (Days 15–35) and near 01:00 at the end (Days 55–80). The black pluses are for each day for each year, the red diamonds are the 12-year average. For the WACCM model, the solid line is an 8-year model average of the case with polar mesospheric clouds included; the dashed line is the equivalent no polar mesospheric cloud case. SABER = Sounding of the Atmosphere using Broadband Emission Radiometry; WACCM = Whole Atmosphere Community Climate Model.

SH PMC season in WACCM is delayed by almost a month relative to SOFIE. This is consistent with the same discrepancy seen in the comparison of WACCM-PMC H with SABER.

Finally, Figure 6 shows a comparison of July (left panel) and January (right panel) averaged water vapor from SOFIE and WACCM-PMC for both model cases, with and without PMC. The SOFIE data are shown both as individual years (dots) and an average as with Figure 5; the WACCM-PMC results are 8-year averages. The model case with PMCs (red curves) shows a pronounced layer of enhanced water vapor near .01 hPa and a clear region of dehydration in the .002–.005 hPa region. At least in the NH, the model does tend to overestimate the magnitude of the sublimated layer and the degree of dehydration. Data from the Michelson Interferometer for Passive Atmospheric Sounding instrument also show much less dehydration than the 2–3 ppmv suggested by the model (cf. Garcia-Comas et al., 2016, their Figure 10). A model overestimate of dehydration has been seen in other simulations (e.g., Bardeen et al., 2010; von Zahn & Berger, 2003), so we conducted a study to investigate whether increased eddy diffusion would smear out the H_2O profile and thus reduce both the dehydration and the sublimation. Our approach to test this was to change the Prandtl number (Pr) from 4 to 2. Since Pr varies inversely with K_{zz} , this has the effect of doubling the eddy mixing (Garcia et al., 2017). However, as seen by comparing the solid curve ($Pr = 4$) and the red dashed curve ($Pr = 2$) in the figure, this had only a small effect. Given that the IWC and H variations were in such good agreement with SOFIE and SABER, respectively, it is somewhat puzzling why the model overestimates the dehydration and underestimates the sublimation. We note that Michelson Interferometer for Passive Atmospheric Sounding data (Garcia-Comas et al., 2016) showed an H_2O anomaly similar to SOFIE, or even less: about 0.5 ppmv depletion from 85–95 km and an enhancement of around 1.4 ppmv at 80 km (their Figure 10). Thus, the WACCM overestimate seems to be of some generality. To explain why models overestimate the H_2O anomaly, Bardeen et al. (2010) have suggested that subgrid scale gravity waves, not represented in the model, could cause sublimation to occur over

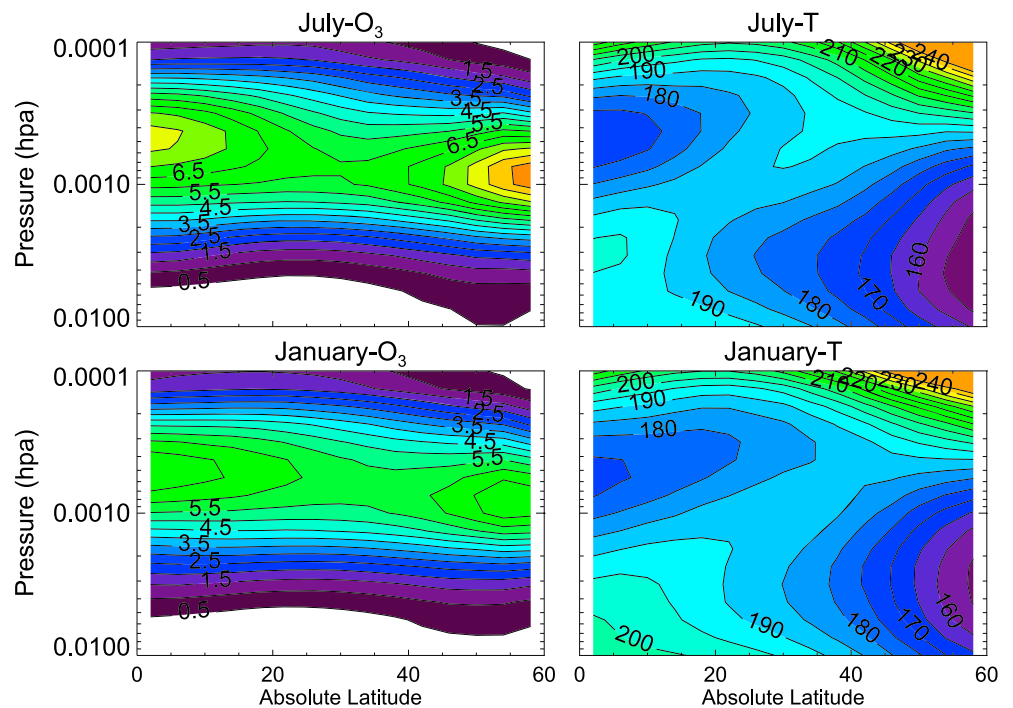


Figure 8. Nighttime summer Sounding of the Atmosphere using Broadband Emission Radiometry ozone and temperature for NH (top) and SH (bottom). The data represent 12-year averages where the period of averaging covers an 8- to 10-day period in early July for the NH and early January for the SH where the solar zenith angle at the Sounding of the Atmosphere using Broadband Emission Radiometry tangent point is greater than 98° . The exact dates tend to vary from year to year due to orbital changes.

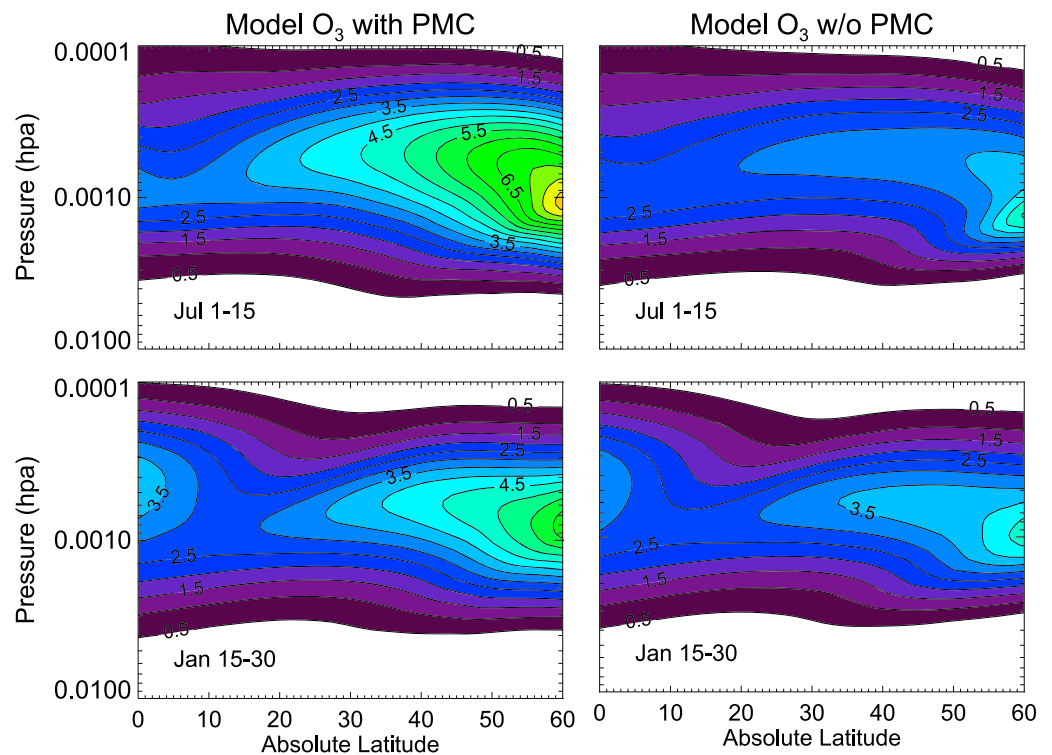


Figure 9. Nighttime zonal average model ozone for a calculation with (left column) and without (right column) PMCs included. Top row is an 8 model year average for 1–15 July, bottom is for 15–30 January. PMC = polar mesospheric cloud.

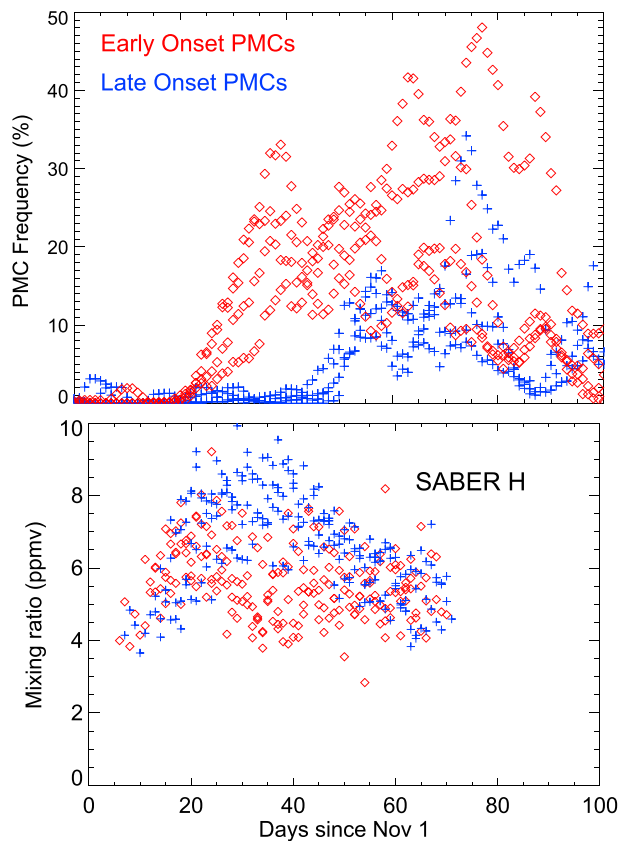


Figure 10. Comparison of PMC frequencies observed by CIPS to H observed by SABER. (top) Average Aeronomy of Ice in the Mesosphere CIPS frequencies from 65 to 75°S for four PMC seasons with the earliest onsets (red diamonds: 2009–2010, 2012–2013, 2013–2014, and 2016) and with the latest onsets (blue crosses: 2007–2008, 2010–2011, 2011–2012, and 2015–2016). A 7-day running mean has been applied. (bottom) Daily averaged SABER H for 70°S and 0.00056 hPa. The same years and same color scheme is used as with the CIPS data. PMC = polar mesospheric cloud; SABER = Sounding of the Atmosphere using Broadband Emission Radiometry; CIPS = Cloud Imaging and Particle Size.

a broader range of altitudes, thus smoothing out the narrow layer seen in the models. This remains a topic for future study.

In summary, this section demonstrated that the model estimates of IWC, H , and H_2O compare reasonably well with observations. These results support the suggestion by Siskind et al. (2008) that the decrease of H during the summer near the mesopause is due to the sequestration of water vapor by PMC formation. A new result is that this effect on H is seen at lower latitudes, outside the PMC formation region. This is postulated to be due to the equatorward mean meridional circulation.

3.2. Nighttime Ozone

Given the well-known link between odd hydrogen and odd oxygen (Brasseur & Solomon, 2005), we would expect an increase in ozone where the H is depleted. We can see this most easily by looking at nighttime conditions. The reason for using nighttime data is that the equilibrium equation for the ozone distribution does not depend upon photolysis and more clearly shows the anticorrelation with atomic hydrogen. Equation (4) of Smith et al. (2014; labeled equation (1) here) approximates the nighttime ozone abundance as

$$O_3 = \frac{(k_1[O][O_2][M])}{(k_2[H] + k_3[O])} \quad (1)$$

Equation (1) shows that there are two loss terms, from reaction with H and O . However, evaluating the denominator using standard JPL rates (Sander et al., 2011; $k_2 = 1.4 \times 10^{-10} \exp(-470/T)$ and $k_3 = 8.0 \times 10^{-12} \exp(-2060/T)$) for typical mesospheric temperatures near 190 km (e.g., $T = 150$ K) and representative H and O densities (e.g., $H = 5 \times 10^7 \text{ cm}^{-3}$ and $O = 4 \times 10^{11} \text{ cm}^{-3}$) we see that the $k_2[H]$ term is well over an order of magnitude greater than the $k_3[O]$ term. Thus, O_3 should vary inversely with H at night.

We investigate this relationship using nighttime ozone and temperature data from SABER. Nighttime data are preferable both because it flows naturally from equation (1) above, but also because it avoids having to consider zenith angle effects, which change the O/O_3 partitioning during the day. Of course, periods of nighttime at middle to high latitudes are limited in summer; however, there are two periods during the poleward yaw (cf.

Figure 2) where SABER samples latitudes as high as 55–60° and when the solar zenith angle is greater than 98° at the tangent point of the limb sample. The first is about 10 days right after the yaw, where local times are sampled near 23:00, and the second is a period of about 8–10 days after 1 July (for the NH) and 1 January (for the SH) where local times near 01:00 are sampled. Figure 7 shows the time variation of these data, compared with WACCM/PMC, in a format similar to Figure 2. The figure shows that at the beginning of the period (Days 15–35), the ozone is decreasing in both SABER and the model. This is due to the increasing H as seen in Figure 2. Then once the PMC season begins, the model shows a significant increase in ozone. SABER shows that in the second nighttime period (Days 55–80), the ozone abundance is clearly larger by about 1–3 ppmv than on Days 30–35. Admittedly, the enhancement is less than in the model; this may reflect the overestimate of the H_2O dehydration discussed above. However, it is clear that the ozone has increased.

Although the observed ozone increase at 55–60° is somewhat smaller than in the model, it is significant enough to create a local maximum in abundance. Figure 8 shows zonal average SABER ozone and temperature for early July and early January. It can be seen that there are two regional ozone maxima: near the equator and 60°. The tropical ozone maximum has been discussed previously (Smith et al., 2008, 2013) and lines up nicely with the occurrence of low temperatures at the tropical mesopause between $p = 1 \times 10^{-3}$ and 3×10^{-4} hPa. The anticorrelation between ozone and temperature is well known and stems directly from the temperature dependencies of reactions k_1 , k_2 , and k_3 in equation (1) (i.e., k_1 varies inversely with temperature, while k_2 and k_3 vary directly with temperature). The other ozone maximum, near 60° latitude N/S, has not previously

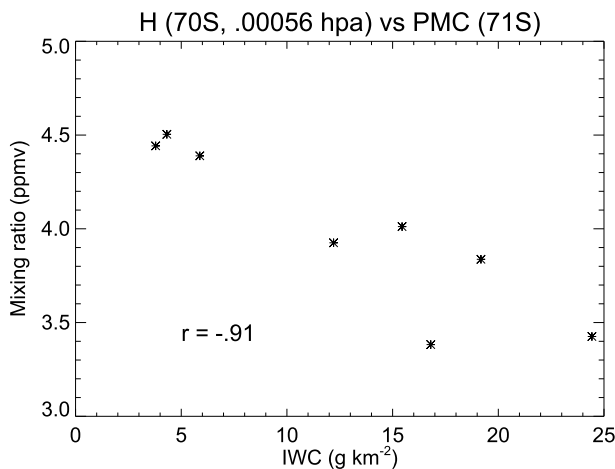


Figure 11. Scatterplot of calculated H mixing ratio (70°S , $.00056\text{ hPa}$) versus calculated column IWC (lat = 71°S) for 1–15 January. The correlation coefficient is indicated. PMC = polar mesospheric cloud; IWC = ice water content.

been identified and is vertically displaced from the temperature minimum at the mesopause. In this case, the maximum in nighttime ozone corresponds to where the hydrogen is depleted from PMC formation.

Figure 9 shows the WACCM-PMC simulations both with and without PMCs for midnight for the periods 1–15 July (top) and 15–30 January (bottom). Note the SH results that we show are later in the summer season compared with the NH to account for the model delay in the SH PMC onset. Comparing Figures 8 and 9, it is clear that the model simulation with PMCs gives an ozone maximum near 60°N/S that agrees much better with SABER than the model simulation without PMCs. This confirms that the ozone maximum is due to the reduced H from PMC formation.

It is also worth noting that neither simulation captures the tropical maximum in ozone that is so evident in SABER. It has been shown that in general, models underestimate mesospheric ozone (Siskind, Stevens, Englert, et al., 2013; Smith et al., 2014). Further, in this case, a contribution to this model deficit is most likely because the model temperatures are higher (about 190–200 K) near $p = 5 \times 10^{-3}\text{ hPa}$ than observations indicate (about 160–170 K, not shown), possibly due to an underestimate by WACCM of the diurnal tide. Given the aforementioned strong anticorrelation of ozone with temperature, a warm bias of 30 K in the model can easily lead to the differences seen at tropical latitudes.

3.3. Interannual Variability

Here we further consider the interannual variability in the summertime H decrease seen by SABER in the SH. As we have already discussed, the onset of the PMC season in the SH will vary based upon the timing of the breakdown of the stratospheric polar vortex, which can vary by up to a month. Figure 10 shows how this variability in PMC formation is mirrored in the atomic hydrogen. The top panel of the figure shows the PMC occurrence frequency as measured by CIPS for a total of eight seasons. Four seasons (2009–2010, 2012–2013, 2013–2014, and 2016–2017) are considered *early onset* and are marked with red diamonds. Four seasons (2007–2008, 2010–2011, 2011–2012, and 2015–2016) are considered *late onset* and are marked with blue crosses. The CIPS data clearly show the 1 month difference between early and late onset. Karlsson et al. (2011) have provided an interpretation of this variability in terms of the timing of the breakdown of the stratospheric polar vortex. The bottom panel of Figure 10 shows the concomitant daily averaged SABER H for the same eight seasons, marked with the same colors and symbols as the CIPS data. It is clear that years with early PMC onset show a rapid decrease in H such that values near 4 ppmv are seen by early December (Day 35). By contrast, when PMC formation, and associated dehydration, are delayed, H continues to increase to values over 8 ppmv in early December, before subsequently declining. Thus, the large scatter in the SABER H at 70°S relative to

70°N that was shown in Figure 2 is seen to be the result of the combination of the two populations, early and late PMC onset.

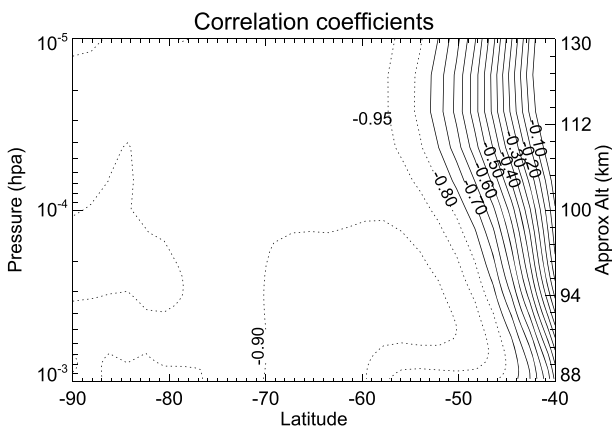


Figure 12. Correlation of calculated H mixing ratio over the indicated latitude and pressure range versus the calculated column ice water content shown in Figure 10 (71°S , 1–15 January).

While the WACCM results do not display a discrete division into early versus late in the PMC onset as do the observations, the results in Figure 10 do imply that at the beginning of the PMC season, there should be an anticorrelation between IWC and H in the lower thermosphere. We can use the model to test this hypothesis and to see how broadly this pattern extends. Note that we use the period of 1–15 January as the definition of the beginning of the SH model PMC season recognizing, as discussed earlier, that this is about a month later than observed. Figure 11 shows that modeled atomic hydrogen from 70°S and 0.0006 hPa ($94\text{--}95\text{ km}$) does clearly anticorrelate ($r = -0.91$) with the model IWC at 71°S at the beginning of the SH PMC season for the 8 model years. Figure 12 shows this anticorrelation between the modeled PMC ice column mass at 70°S (1–15 January) and the modeled atomic hydrogen exists over a large fraction of the SH (poleward of 45°) and extends up to the model lid at 140 km. This provides additional intriguing evidence that PMC formation can influence the composition of the atmosphere up into the thermosphere. Since, as discussed

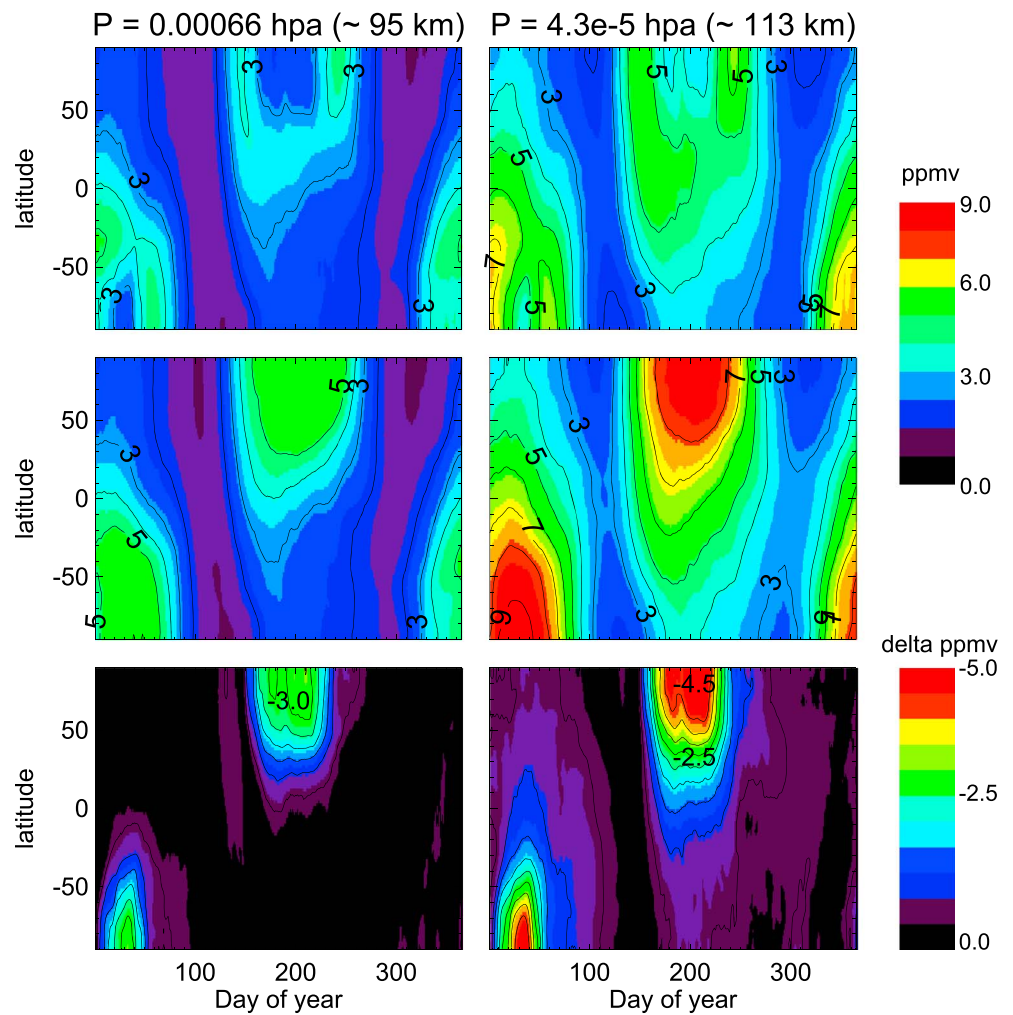


Figure 13. Model thermospheric hydrogen (daily average over 8 model years) for the mesopause region (left column) and lower thermosphere (right column). The top row is for the model that includes the PMC parameterization, the middle row is for the model without PMCs, and the bottom is the difference (with PMCs minus without PMCs). The difference is negative reflecting the depletion in H due to PMCs. PMC = polar mesospheric cloud.

above, the onset of the SH PMC season is known to be the result of stratospheric dynamic variability (Karlsson et al., 2011), this suggests a heretofore undocumented pathway for stratospheric-thermospheric coupling.

3.4. Extension Into the Lower Thermosphere: A Summertime Hydrogen Hole

Given the evidence from Figure 12 that the timing of the onset of the PMC season correlates with the abundance of atomic hydrogen up into the lower thermosphere, it is useful to quantify the possible effects of PMC formation on thermospheric hydrogen distribution more generally. While these model results above 100 km cannot be directly validated with observations, they may be useful constraints to compare with thermospheric hydrogen measurements such as those described by Waldrop and Paxton (2013). Figure 13 shows the calculated hydrogen as a function of latitude and time of year for two pressure levels. The top row represents the WACCM-PMC simulation with PMCs, the middle row is the control case without PMCs, and the bottom row shows the difference. The figure shows that in general, lower thermospheric hydrogen maximizes at middle to high latitudes each summer. As discussed by Qian et al. (2018), this is due to the seasonal upwelling of water vapor up to the mesopause combined with photodissociation during the long summer days. Interestingly, however, superimposed upon this summertime increase is a pronounced biteout of H from PMC dehydration. Thus, the general seasonal variation in WACCM-PMC H , which compared favorably with SABER at 0.0006 hPa, is seen to project relatively unchanged into the lower thermosphere. The bottom row shows the effect of the PMC dehydration at 113 km can extend to latitudes equatorward of 30° even up at 113 km. We note that the physical mechanism whereby the dehydration spreads equatorward is likely different at 113 km than at 90 km.

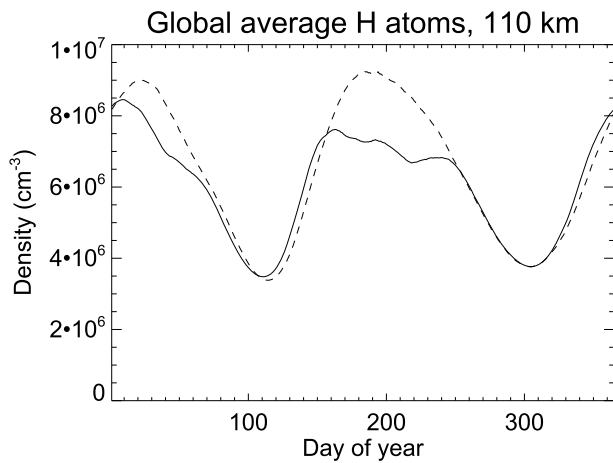


Figure 14. Global average, area weighted, hydrogen density at 110 km from Whole Atmosphere Community Climate Model-PMC. The solid curve is the calculation with PMCs; the dashed curve is for the model without PMCs. PMC = polar mesospheric cloud.

This is because it is generally understood that the mean meridional circulation reverses and flows winter to summer above 95–100 km (Qian et al., 2017; Smith et al., 2011). Qian et al. (2018) emphasize the role of the diffusive separation velocity, which depends upon the ratio of the constituent mean mass and the background atmospheric mass. As they note, this ratio is largest for atomic hydrogen. The simulations they present show that this diffusive velocity maps the mesospheric seasonal cycle of atomic hydrogen (i.e., summer maximum and equatorward transport) up to as high as 130 km. The equatorward transport of the PMC depletion in the lower thermosphere seen in Figure 13 is consistent with the Qian et al. (2018) results.

Figure 14 shows the modeled global mean (area weighted) H abundance at 110 km throughout the year, which emphasizes the peaks at solstice. It further shows that the PMC biteouts are noticeable even on a globally averaged basis. On an annually integrated basis, the difference between the two curves is about 7%. Thus, PMCs, at least in the model, reduce the amount of hydrogen entering the thermosphere by this amount.

4. Conclusions

We have shown how a general circulation model with a parameterization of PMC formation can be used to study the effects of PMCs on the composition of the mesosphere and lower thermosphere. We have shown how dehydration due to PMC ice condensation can have significant effects on the chemical composition of the summer mesosphere, even propagating up into the lower thermosphere. Among the manifestations of this dehydration is a seasonal decrease in H near the mesopause. The year-to-year variability of this decrease is reflected in the observed variation in the onset of the SH PMC season. The H decrease is also seen to spread to lower latitudes and to higher altitudes, consistent with the currently understood behavior of the zonal mean circulation combined with rapid vertical diffusion of H above 95–100 km. Because of HO_x - O_x anticorrelation, the depletion of H creates a nighttime ozone maximum in the midlatitude summer mesopause region. In the lower thermosphere, effects of PMC freeze drying are seen to reduce the hydrogen density by about 7%. Since thermospheric hydrogen ultimately flows upward into the exosphere (Yung et al., 1989), in principle, at least, PMCs might have a small effect on escape of hydrogen from the Earth's atmosphere.

References

- Bailey, S. M., Merkel, A. W., Thomas, G. E., & Carstens, J. N. (2005). Observations of polar mesospheric clouds from the SNOE satellite. *Journal of Geophysical Research*, *110*, D13203. <https://doi.org/10.1029/2004JD005422>
- Bailey, S. M., Thomas, G. E., Rusch, D. W., Merkel, A. W., Jeppesen, C., Carstens, J. N., et al. (2009). Phase functions of polar mesospheric cloud ice as observed by the CIPS instrument on the AIM satellite. *Journal of Atmospheric and Solar–Terrestrial Physics*, *71*(3–4), 373–380.
- Bardeen, C. G., Marsh, D. R., Jackman, C. H., Hervig, M. E., & Randall, C. E. (2016). Impact of the January 2012 solar proton event on polar mesospheric clouds. *Journal of Geophysical Research: Atmospheres*, *121*, 9165–9173. <https://doi.org/10.1002/2016JD024820>
- Bardeen, C. G., Toon, O. B., Jensen, E. J., Hervig, M. E., Randall, C. E., Benze, S., et al. (2010). Numerical simulations of the three-dimensional distribution of polar mesospheric clouds and comparisons with Cloud Imaging and Particle Size (CIPS) experiment and the Solar Occultation for Ice Experiment (SOFIE) observations. *Journal of Geophysical Research*, *115*, D10204. <https://doi.org/10.1029/2009JD012451>
- Benze, S., Randall, C. E., Karlsson, B., Harvey, V. L., DeLand, M. T., Thomas, G. E., & Shettle, E. P. (2012). On the onset of polar mesospheric cloud seasons as observed by SBUV. *Journal of Geophysical Research*, *117*, D07104. <https://doi.org/10.1029/2011JD017350>
- Brasseur, G., & Solomon, S. (2005). *Aeronomy of the middle atmosphere* (3rd ed.). Netherlands: Springer. 644.
- DeLand, M. T., Shettle, E. P., Thomas, G. E., & Olivero, J. J. (2003). Solar backscattered ultraviolet (SBUV) observations of polar mesospheric clouds (PMC) over two solar cycles. *Journal of Geophysical Research*, *108*(D8), 8445. <https://doi.org/10.1029/2002JD002358>
- DeLand, M. T., & Thomas, G. E. (2015). Updated PMC trends derived from SBUV data. *Journal of Geophysical Research: Atmospheres*, *120*, 2140–2166. <https://doi.org/10.1002/2014JD022253>
- France, J. A., Randall, C. E., Lieberman, R. S., Harvey, V. L., Eckermann, S. D., Siskind, D. E., et al. (2018). Local and remote planetary wave effects on Polar Mesospheric Clouds in the Northern Hemisphere in 2014. *Journal of Geophysical Research: Atmospheres*, *123*, 5149–5162. <https://doi.org/10.1029/2017JD028224>
- Garcia, R. R. (1989). Dynamics, radiation and photochemistry in the mesosphere: Implications for the formation of noctilucent clouds. *Journal of Geophysical Research*, *94*, 14,605–14,615.
- Garcia, R. R., Marsh, D. R., Kinnison, D. E., Boville, B. A., & Sassi, F. (2007). Simulation of secular trends in the middle atmosphere, 1950–2005. *Journal of Geophysical Research*, *112*, D09301. <https://doi.org/10.1029/2006JD007485>
- Garcia, R. R., Smith, A. K., Kinnison, D. E., Cámara, Á., & Murphy, D. J. (2017). Modification of the gravity wave parameterization in WACCM: Motivation and results. *Journal of the Atmospheric Sciences*, *74*, 275–291. <https://doi.org/10.1175/JAS-D-16-0104.1>

Acknowledgments

D.E.S. and A.W.M. acknowledge support from NASA/HSR grant NNH14AX50L. Additional support was provided by the NASA AIM Small Explorer program (through Interagency Purchase Request S50029G to N.R.L. and through contract NAS5-03132) and the NASA/TIMED SABER project (through Interagency Purchase Request NNG17PX04I to N.R.L.). Resources supporting this work were provided by the NASA High-End Computing (HEC) Program through the NASA Advanced Supercomputing (NAS) Division at the Ames Research Center. The SABER and SOFIE data are available from www.gats-inc.com/projects.html. The CIPS data are available from <http://lasp.colorado.edu/aim/>. The WACCM-PMC model results, for both Pr = 2 and 4, are archived as Python-readable IDL save files and are accessible at <https://map.nrl.navy.mil> (cd to map/pub/nrl/waccmpmc).

- García-Comas, M., Lopez-Puertas, M., Funke, B., Jurado-Navarro, A. A., Gardini, A., Stiller, G. P., et al. (2016). Measurements of global distributions of polar mesospheric clouds during 2005–2012 by MIPAS/Envisat. *Atmospheric Chemistry and Physics*, *16*(11), 6701–6719. <https://doi.org/10.5194/acp-16-6701-2016>
- Gordley, L. L., Hervig, M. E., Fish, C., Russell, J. M. III, Bailey, S., Cook, J., et al. (2009). The solar occultation for ice experiment. *Journal of Atmospheric and Solar-Terrestrial Physics*, *71*, 300–315. <https://doi.org/10.1016/j.jastp.2008>
- Hervig, M. E., Berger, U., & Siskind, D. E. (2016). Decadal variability in PMCs and implications for changing temperature and water vapor in the upper mesosphere. *Journal of Geophysical Research: Atmospheres*, *121*, 2383–2392. <https://doi.org/10.1002/2015JD024439>
- Hervig, M. E., Gordley, L. L., Stevens, M., Russell, J. M., Bailey, S., & Baumgarten, G. (2009). Interpretation of SOFIE PMC measurements: cloud identification and derivation of mass density, particle shape, and particle size. *Journal of Atmospheric and Solar-Terrestrial Physics*, *71*, 316–330. <https://doi.org/10.1016/j.jastp.2008.07.009>
- Hervig, M. E., McHugh, M., & Summers, M. E. (2003). Water vapor enhancement in the polar summer mesosphere and its relationship to polar mesospheric clouds. *Geophysical Research Letters*, *30*(20), 2041. <https://doi.org/10.1029/2003GL018089>
- Hervig, M. E., & Siskind, D. (2006). Decadal and inter-hemispheric variability in polar mesospheric clouds, water vapor and temperature. *Journal of Atmospheric and Solar-Terrestrial Physics*, *68*, 30–41.
- Hervig, M. E., Siskind, D. E., Bailey, S. M., & Russell, J. M. III (2015). The influence of PMCs on water vapor and drivers behind PMC variability from SOFIE observations. *Journal of Atmospheric and Solar-Terrestrial Physics*, *132*, 124–134. <https://doi.org/10.1016/j.jastp.2015.07.010>
- Hervig, M. E., Siskind, D. E., Stevens, M. H., & Deaver, L. E. (2013). Inter-hemispheric comparison of PMCs and their environment from SOFIE observations. *Journal of Atmospheric and Solar-Terrestrial Physics*, *104*, 285–298. <https://doi.org/10.1016/j.jastp.2012.10.013>
- Hervig, M. E., & Stevens, M. H. (2014). Interpreting the 35 year SBUV/PMC record with SOFIE observations. *Journal of Geophysical Research: Atmospheres*, *119*, 12,689–12,705. <https://doi.org/10.1002/2014JD021923>
- Karlsson, B., Kornich, H., & Gumbel, J. (2007). Evidence for interhemispheric stratosphere-mesosphere coupling derived from noctilucent cloud properties. *Geophysical Research Letters*, *34*, L18606. <https://doi.org/10.1029/2007GL030282>
- Karlsson, B., Randall, C. E., Benze, S., Mills, M., Harvey, V. L., Bailey, S. M., & Russell, J. M. III (2009). Intra-seasonal variability of polar mesospheric clouds due to inter-hemispheric coupling. *Geophysical Research Letters*, *36*, L20802. <https://doi.org/10.1029/2009GL040348>
- Karlsson, B., Randall, C. E., Shepherd, T. G., Harvey, V. L., Lumpe, J., Nielsen, K., et al. (2011). On the seasonal onset of polar mesospheric clouds and the breakdown of the stratospheric polar vortex in the Southern Hemisphere. *Journal of Geophysical Research*, *116*, D18107. <https://doi.org/10.1029/2011JD015989>
- Lubken, F.-J., Berger, U., & Baumgarten, V. (2009). Stratospheric and solar cycle effects on long-term variability of mesospheric ice clouds. *Journal of Geophysical Research*, *114*, D00106. <https://doi.org/10.1029/2009JD012377>
- Lumpe, J. D., Bailey, S. M., Carstens, J. N., Randall, C. E., Rusch, D. W., Thomas, G. E., et al. (2013). Retrieval of polar mesospheric cloud properties from CIPS: Algorithm description, error analysis and cloud detection sensitivity. *Journal of Atmospheric and Solar-Terrestrial Physics*, *104*, 167–196. <https://doi.org/10.1016/j.jastp.2013.06.007>
- Merkel, A. W., Marsh, D. R., Gettleman, A., & Jensen, E. J. (2009). On the relationship of polar mesospheric cloud ice water content, particle radius and mesospheric temperature and its use in multi-dimensional models. *Atmospheric Chemistry and Physics*, *9*, 8889–8901.
- Megner, L., Siskind, D. E., Rapp, M., & Gumbel, J. (2008). Global and temporal distribution of meteoric smoke: A two-dimensional simulation study. *Journal of Geophysical Research*, *113*, D03202. <https://doi.org/10.1029/2007JD009054>
- Merkel, A. W., Rusch, D. W., Palo, S. E., Russell, J. M. III, & Bailey, S. M. (2009). Mesospheric planetary wave effects on global PMC variability inferred from AIM-CIPS and TIMED-SABER for the northern summer 2007 PMC season. *Journal of Atmospheric and Solar-Terrestrial Physics*, *71*, 381–391. <https://doi.org/10.1016/j.jastp.2008.12.001>
- Mlynczak, M. G., Hung, L. A., Marshall, B. T., Mertens, C. J., Marsh, D. R., Smith, A. K., et al. (2013). Atomic hydrogen in the mesopause region derived from SABER. *Journal of Geophysical Research: Atmospheres*, *119*, 3516–3526. <https://doi.org/10.1002/2013JD021263>
- Mlynczak, M. G., Hunt, L. A., Russell, J. M. III, & Marshall, B. T. (2018). Updated SABER night atomic oxygen and implications for SABER ozone and atomic hydrogen. *Geophysical Research Letters*, *45*, 5735–5741. <https://doi.org/10.1029/2018GL077377>
- Qian, L., Burns, A. G., Solomon, S. S., Smith, A. K., McInerney, J. M., Hunt, L. A., et al. (2018). Temporal variability of atomic hydrogen from the mesopause to the upper thermosphere. *Journal of Geophysical Research: Space Physics*, *123*, 1006–1017. <https://doi.org/10.1002/2017JA024998>
- Qian, L., Burns, A., & Yue, J. (2017). Evidence of the lower thermospheric winter-to-summer circulation from SABER CO₂ observations. *Geophysical Research Letters*, *44*, 10,100–10,107. <https://doi.org/10.1002/2017GL075643>
- Remsberg, E. E., Marshall, B. T., García-Comas, M., Krueger, D., Lingenfeller, G. S., Martín-Torres, J., Mlynczak, M. G., et al. (2008). Assessment of the quality of the Version 1.07 temperature-versus-pressure profiles of the middle atmosphere from TIMED/SABER. *Journal of Geophysical Research*, *113*, D17101. <https://doi.org/10.1029/2008JD010013>
- Richter, J., Sassi, H. F., & García, R. R. (2010). Towards a physically based gravity wave source parameterization. *Journal of the Atmospheric Sciences*, *67*, 136–156. <https://doi.org/10.1179/2009JAS3112.1>
- Rong, P. P., Russell, J. M. III, Gordley, L. L., Hervig, M. E., Deaver, L., Bernath, P. F., & Walker, K. A. (2010). Validation of v1.022 mesospheric water vapor observed by the solar occultation for ice experiment on the Aeronomy of Ice in the Mesosphere satellite. *Journal of Geophysical Research*, *115*, D24314. <https://doi.org/10.1029/2010JD014269>
- Rong, P. P., Russell, J. M. III, Mlynczak, M. G., Remsberg, E. E., Marshall, B. T., Gordley, L. L., & López-Puertas, M. (2009). Validation of Thermosphere Ionosphere Mesosphere Energetics and Dynamics/Sounding of the Atmosphere using Broadband Emission Radiometry (TIMED/SABER) v1.07 ozone at 9.6 mm in altitude range 15–70 km. *Journal of Geophysical Research*, *114*, D04306. <https://doi.org/10.1029/2008JD010073>
- Rusch, D. W., Thomas, G. E., McClintock, W., Merkel, A. W., Bailey, S. M., Russell, J. M. III, et al. (2009). The cloud imaging and particle size experiment on the Aeronomy of Ice in the Mesosphere mission: Cloud morphology for the Northern 2007 season. *Journal of Atmospheric and Solar-Terrestrial Physics*, *71*, 356–364. <https://doi.org/10.1016/j.jastp.2008.11.005>
- Sander, S. P., Abbatt, J. P. D., Barker, J. R., Burkholder, J. B., Friedl, R. R., Golden, D. M., et al. (2011). *Chemical kinetics and photochemical data for use in atmospheric studies: Evaluation number 17* (pp. 10–6). Pasadena, CA: JPL Publication.
- Shettle, E. P., DeLand, M. T., Thomas, G. E., & Olivero, J. J. (2009). Long term variations in the frequency of polar mesospheric clouds in the Northern Hemisphere from SBUV. *Geophysical Research Letters*, *36*, L02803. <https://doi.org/10.1029/2008GL036048>
- Siskind, D. E., Allen, D. R., Randall, C. E., Harvey, V. L., Hervig, M. E., Lumpe, J., et al. (2015). Extreme stratospheric springs and their consequences for the onset of polar mesospheric clouds. *Journal of Atmospheric and Solar-Terrestrial Physics*, *132*, 74–81. <https://doi.org/10.1016/j.jastp.2015.06.014>
- Siskind, D. E., Eckermann, S. D., McCormack, J. P., Alexander, M. J., & Bacmeister, J. T. (2003). Hemispheric differences in the temperature of the summertime stratosphere and mesosphere. *Journal of Geophysical Research*, *108*(D2), 4051. <https://doi.org/10.1029/2002JD002095>

- Siskind, D. E., Hervig, M. E., Gumbel, J., & Stevens, M. H. (2007). Polar mesospheric cloud mass and ice mass budget: 3. Application of a coupled ice-chemistry-dynamics model and comparison with observations. *Journal of Geophysical Research*, *112*, D08303. <https://doi.org/10.1029/2006JD007499>
- Siskind, D. E., Marsh, D. R., Mlynczak, M. G., Martin-Torres, F. J., & Russell, J. M. (2008). Decreases in atomic hydrogen over the summer pole: Evidence for dehydration from polar mesospheric clouds? *Geophysical Research Letters*, *35*, L13809. <https://doi.org/10.1029/2008GL033742>
- Siskind, D. E., & McCormack, J. P. (2014). Summer mesospheric warmings and the quasi 2 day wave. *Geophysical Research Letters*, *41*, 717–722. <https://doi.org/10.1002/2013GL058875>
- Siskind, D. E., Stevens, M. H., Englert, C. R., & Mlynczak, M. G. (2013). Comparison of a photochemical model with observations of mesospheric hydroxyl and ozone. *Journal of Geophysical Research: Atmospheres*, *118*, 195–207. <https://doi.org/10.1029/2012JD017971>
- Siskind, D. E., Stevens, M. H., Hervig, M. E., & Randall, C. E. (2013). Recent observations of high mass density polar mesospheric clouds: A link to space traffic? *Geophysical Research Letters*, *40*, 2813–2817. <https://doi.org/10.1002/grl.50540>
- Siskind, D. E., Stevens, M. H., Hervig, M., Sassi, F., Hoppel, K., Englert, C. R., & Kochenash, A. J. (2011). Consequences of recent Southern Hemisphere winter variability on polar mesospheric clouds. *Journal of Atmospheric and Solar-Terrestrial Physics*, *73*, 2013–2001.
- Smith, A. K., Espy, P., Lopez-Puertas, M., & Tweedy, O. (2018). Spatial and temporal structure of the tertiary ozone maximum in the polar winter mesosphere. *Journal of Geophysical Research: Atmospheres*, *123*, 4373–4389. <https://doi.org/10.1029/2017JD028030>
- Smith, A. K., Garcia, R. R., Marsh, D. R., Kinnison, D. E., & Richter, J. H. (2010). Simulations of the response of mesospheric circulation and temperature to the Antarctic ozone hole. *Geophysical Research Letters*, *37*, L22803. <https://doi.org/10.1029/2010GL045255>
- Smith, A. K., Garcia, R. R., Marsh, D. R., & Richter, J. H. (2011). WACCM simulations of the mean circulation and trace species transport in the winter mesosphere. *Journal of Geophysical Research*, *116*, D02115. <https://doi.org/10.1029/2011JD016083>
- Smith, A. K., Harvey, V. L., Mlynczak, M. G., Funke, B., Garcia-Comas, M., Hervig, M., et al. (2013). Satellite observations of ozone in the upper mesosphere. *Journal of Geophysical Research: Atmospheres*, *118*, 5803–5821. <https://doi.org/10.1002/jgrd.50445>
- Smith, A. K., López-Puertas, M., Funke, B., García-Comas, M., Mlynczak, M. G., & Holt, L. A. (2014). Nighttime ozone variability in the high latitude winter mesosphere. *Journal of Geophysical Research: Atmospheres*, *119*, 13,547–13,564. <https://doi.org/10.1002/2014JD021987>
- Smith, A. K., Marsh, D., Russell, J. M. III, Mlynczak, M. G., Martin-Torres, F. J., & Kyrola, E. (2008). Satellite observations of high nighttime ozone at the equatorial mesopause. *Journal of Geophysical Research*, *113*, D17312. <https://doi.org/10.1029/2008JD010066>
- Stevens, M. H., Englert, C. R., DeLand, M. T., & Bailey, S. M. (2007). Polar mesospheric cloud mass and the ice budget: 2. Application to satellite data sets. *Journal of Geophysical Research*, *112*, D08205. <http://hdl.handle.net/10919/25301>
- Summers, M. E., Conway, R. R., Englert, C. R., Siskind, D. E., Stevens, M. H., Russell, J. M. III, et al. (2001). Discovery of a water vapor layer in the Arctic summer mesosphere: Implications for polar mesospheric clouds. *Geophysical Research Letters*, *28*, 3601–3604.
- Thuraijajah, B., Thomas, G. E., von Savigny, C., Snow, M., Hervig, M. E., Bailey, S. M., & Randall, C. E. (2017). Solar-induced 27-day variations of polar mesospheric clouds from the AIM SOFIE and CIPS instruments. *Journal of Atmospheric and Solar-Terrestrial Physics*, *162*, 122–135. <https://doi.org/10.1016/j.jastp.8016.09.008>
- von Zahn, U., & Berger, U. (2003). Persistent ice cloud in the midsummer upper mesosphere at high latitudes: Three-dimensional modeling and cloud interactions with ambient water vapor. *Journal of Geophysical Research*, *108*(D8), 8451. <https://doi.org/10.1029/2002JD002409>
- Waldrop, L., & Paxton, L. J. (2013). Lyman alpha airglow emission: Implications for atomic hydrogen geocoronal variability with solar cycle. *Journal of Geophysical Research: Space Physics*, *118*, 5874–5890. <https://doi.org/10.1002/jgra.50496>
- Yung, Y. L., Wen, J.-S., Moses, J. I., Landry, B. M., Allen, M., & Hsu, K.-J. (1989). Escape of hydrogen and deuterium from the terrestrial atmosphere: A quantitative assessment of nonthermal escape fluxes. *Journal of Geophysical Research*, *94*, 14,971–14,989.